water

MDPI

Article

Evaluation of the Effect of Surface Irregularities on the Hydraulic Parameters within Unlined Dam Spillways

Yavar Jalili Kashtiban [1], Ali Saeidi [1,*], Marie-Isabelle Farinas [1] and Javier Patarroyo [2]

[1] Department of Applied Sciences, University of Quebec at Chicoutimi, Chicoutimi, QC G7H 2B1, Canada; yavar.jalilikashtiban1@uqac.ca (Y.J.K.); marie-isabelle_farinas@uqac.ca (M.-I.F.)
[2] Hydro-Québec Production Unité Expertise en Barrages, 75 Boulevard René-Lévesque Ouest, Montréal, QC H2Z 1A4, Canada; patarroyo.javier@hydroquebec.com
* Correspondence: ali_saeidi@uqac.ca

Abstract: Erosional incidents have heightened the necessity of studies regarding rock mass erosion in unlined dam spillways. Enhanced comprehension of hydraulic erodibility necessitates an investigation into the geomechanical and hydraulic aspects of erosional phenomena. Controlled blasting is commonly employed to establish unlined spillways in rock masses, and this process results in irregularities along the spillway surface profile. Recent research has identified key geometric parameters of rock masses that impact erosion in unlined spillways, such as joint opening, dip and dip direction, and joint spacing. However, the effect of spillway surface irregularities on hydraulic parameters remains uncertain. Numerous studies have examined the surface roughness of rock at the millimeter scale within the domain of hydraulic engineering. Despite these efforts, a noticeable gap persists in our understanding of how surface irregularities specifically exert influence over hydraulic parameters. Currently, there is a lack of a clear equation or methodology to incorporate irregularities into hydraulic erosive parameters. The main aim of this study is to show how such irregularities affect the hydraulic parameters. This study is dedicated to emphasizing the importance of considering these irregularities. Building upon the findings obtained, the core aim of this research is to facilitate the formulation of an equation in future investigations that effectively accounts for these irregularities when calculating hydraulic erosive parameters. To assess the significance of surface irregularities in unlined spillways, computational fluid dynamics (CFD) with ANSYS-Fluent software was employed to analyze 25 configurations of spillway surface irregularities and their effects on various factors, including pressure (total, dynamic, and static pressures), shear stress, flow velocity, and energy. The findings indicated that irregularities significantly influenced the hydraulic parameters. Specifically, an increased irregularity height led to a decrease in maximum velocity, total pressure, and shear stress. Conversely, total energy loss increased, amplifying the rock mass's vulnerability to erosion due to these irregularities.

Keywords: dam; hydraulic structures; unlined spillways; erodibility; CFD

Citation: Jalili Kashtiban, Y.; Saeidi, A.; Farinas, M.-I.; Patarroyo, J. Evaluation of the Effect of Surface Irregularities on the Hydraulic Parameters within Unlined Dam Spillways. *Water* **2023**, *15*, 3004. https://doi.org/10.3390/w15163004

Academic Editor: Giuseppe Pezzinga

Received: 19 June 2023
Revised: 9 August 2023
Accepted: 19 August 2023
Published: 20 August 2023

1. Introduction

Unlined dam spillways and other hydraulic safety structures, such as sluice gates, stilling basins, and plunge pools, protect dam infrastructure during high water events. Dam safety can be improved by studying the hydraulic erodibility of these structures and the hydraulic characteristics of flowing water over these constructions. Erodibility, scour, and hydraulic erosion are technical terms related to the erosion that occurs when the hydraulic erosive intensity—erosive capacity of flowing water—exceeds the rock mass resistance [1,2].

Rock mass erosion due to flowing water is a complex phenomenon that can occur instantaneously or over time. Hydraulic erosion mechanisms include brittle failure, fatigue failure, rock block removal, peeling off, and rock block abrasion (Figure 1).

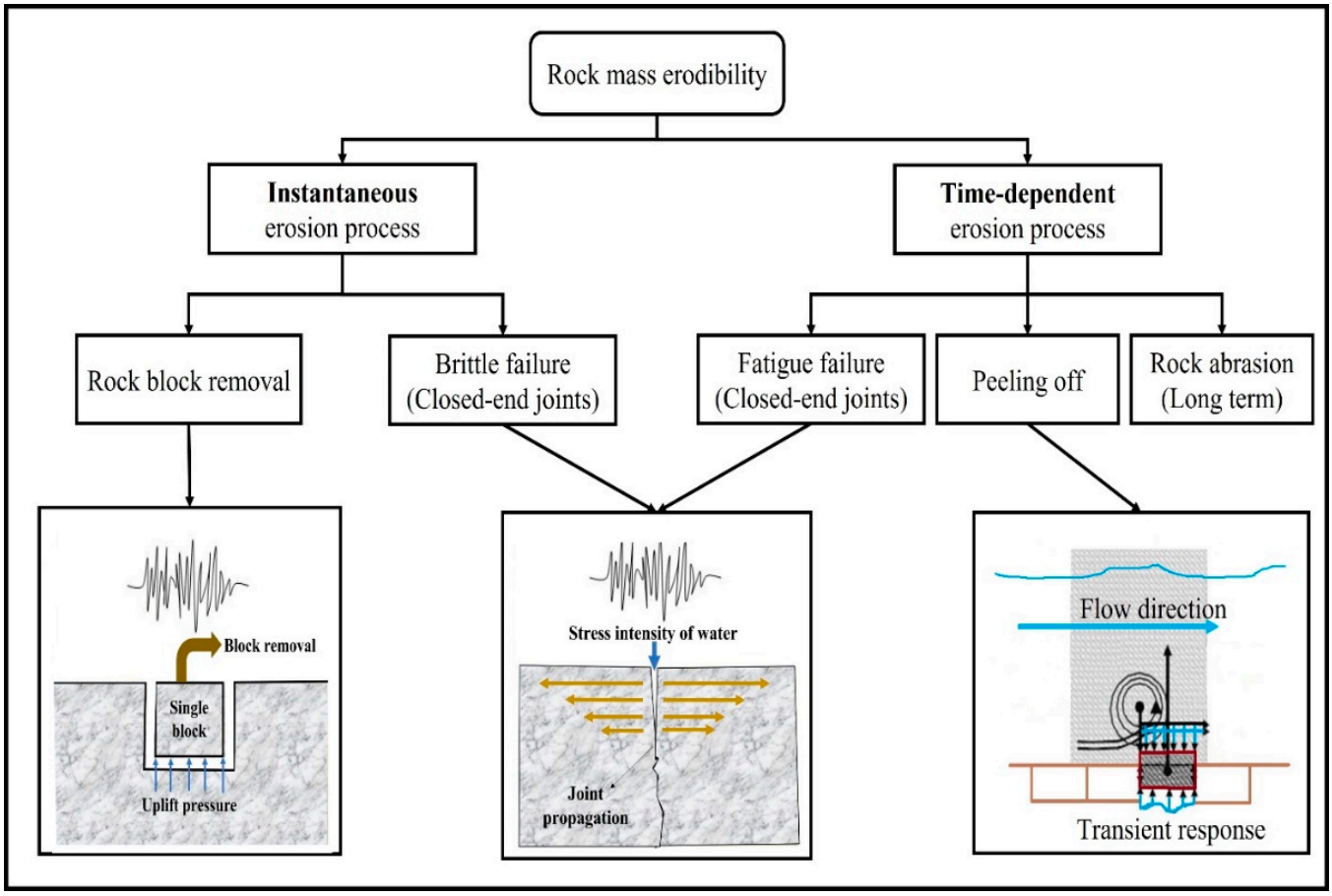

Figure 1. Mechanisms of rock mass erosion [3,4].

Both the hydraulic and rock mass aspects of erosion must be considered. Studying the effect of various geometries of hydraulic constructions on the hydraulic characteristics of flowing water and the effect of geomechanical parameters of the rock mass can improve the analysis of hydraulic erosive parameters [5]. Several investigations have identified the unit stream power dissipation of water (Π_{UD}), water velocity (V), shear stress (τ_b) applied to a rock surface, stress intensity (K_I), and lifting force (F_L) as important hydraulic erosive parameters (Table 1).

Most hydraulic erodibility assessments use an energy dissipation index to reflect the erosive capacity of water because of a lack of an accurate index and the difficulty in determining a specific erosive parameter [6–10]. An energy dissipation index is selected for simplicity, not for accurately representing the hydraulic erosive agent (Table 1). Pells' (2016) analytical methodology appears to be the most reliable among the approaches that use energy dissipation as a hydraulic erosive agent. However, a measure of energy dissipation may not consider all the complexities involved with erosion; for example, spillway geometry (surface profile) and flow modes potentially influence the energy dissipation of water and erosion potential.

Average water velocity is not a representative index of the hydraulic erosive parameter because it depends on the flow channel surface profile, fluid viscosity, and flow nature. Average shear stress along the channel bottom can also be considered a hazard parameter. Nonetheless, it is extremely difficult to resolve all erosion problems within dam spillways by solely considering shear stress, including explaining hydraulic erosion caused by dynamic block removal, brittle failure, or fatigue failure.

Bollaert [11,12] proposed a comprehensive scour model (CSM) using three methods: a comprehensive fracture mechanics (CFM) approach for analyzing erosion in close-ended joints; a dynamic impulsion (DI) approach for analyzing erosion in open-ended joints (single block); and the quasi-steady impulsion (QSI) approach for computing the scoured depth along plunge pool walls. In the CFM, stress intensity (K_I) is considered a hydraulic erosive parameter and is calculated based on the maximum pressure at the plunge pool bottom. Bollaert's DI considers uplift force to be a hydraulic erosive parameter on the basis of impulsion and Newton's second law of thermodynamics. This method ignores the geomechanical and geometric characteristics of the rock mass. In the DI approach, it is assumed that the shear force (F_{sh}) is zero. Bollaert's QSI method determines the forces applied to channel bottoms through the quasi-steady lift force (F_{QSL}) on a protruding block, where the F_{QSL} is dependent on uplift pressure and flow velocity.

Various studies significantly advance our understanding of turbulent fluid dynamics near rough walls. Schmidt and Schumann's 1989 research deeply investigates turbulence within a convective boundary layer (CBL), utilizing large-eddy simulations across various roughness heights. This inquiry integrates finite-difference integration of Navier-Stokes equations, comparing outcomes with empirical data and revealing alignment in vertical mean turbulence metrics, while highlighting differences in horizontal velocity oscillations, pressure perturbations, and dissipation rates [13]. Similarly, Carlotti's 2002 study employs large-eddy simulation (LES), rapid distortion theory, and Eulerian kinematic simulation to explore turbulence properties near the ground, revealing an inner boundary layer within an eddy surface layer, analyzing streamwise structures, spectral signatures, vertical correlations, and spectrum slope modifications [14]. In 1976, Townsend extensively investigates the intricate dynamics underpinning turbulent shear flow, unveiling chaotic behaviors driven by velocity gradients within the fluid [15]. While inspiring, it is vital to recognize that these studies may differ in terms of roughness scales and fluid mechanics contexts from our project. This contrast fuels the development of a tailored, accurate model for our unique project scenario. Together, these scholarly endeavors deepen our understanding of diverse turbulence manifestations.

Existing methods of assessing and predicting hydraulic erodibility are limited by several elements, and these approaches can be used only in specific situations and conditions. Moreover, a unique parameter is lacking to measure the erosive agent of water when assessing rock mass erodibility. For example, numerous equations exist for determining the unit stream power dissipation of water (Π_{UD})—initially developed using internal flow conditions. The concept of stress intensity (K_I) was originally developed for metallurgical analysis [11] and is only used to estimate the probability of joint propagation in intact rocks, not rock masses. When the existing methods are compared (Table 1), the stream power dissipation parameter is the most commonly used; however, spillway geometry is not considered.

Table 1. Existing hydraulic erosive indices.

Hydraulic Erosive Parameter		Equation
Parameter	**Approach**	
Unit stream power dissipation (Π_{UD}) and Stream power dissipation (Π_D)	(Van Schalkwyk 1994) [10] (Annandale 1995) [6] (Pells 2016) [1]	$\Pi_D = \rho \cdot g \cdot q \cdot S$ $\Pi_D = \gamma \cdot q \cdot \Delta E$ $\Pi_{UD} = \rho \cdot g \cdot q \frac{dE}{dx}$
Velocity (V)	(Weisbach 1845, Darcy 1857) [16,17] (Manning et al., 1890) [18]	$V = \sqrt{\frac{8g}{f}} \sqrt{R_H \cdot S_f \cos\theta}$ $V = \frac{1}{n} {R_H}^{2/3} \cdot S^{1/2}$

Table 1. *Cont.*

Hydraulic Erosive Parameter		Equation
Parameter	**Approach**	
Shear stress (τ_b)	(Yunus 2010) [19]	$\overline{\tau}_b = \rho \cdot g \cdot R_H \cdot S \cos\beta$
		$\overline{\tau}_b = \rho \cdot g \cdot R_H \cdot S_f \cos\beta$
	MPM (Khodashenas and Paquier 1999) [20]	$\tau_i = \rho \cdot g \cdot R \cdot J_f$
	(Prasad and Russell 2000) [21]	$\frac{\overline{\tau}_{(b)}}{\rho g h J_f} = (1 - 0.01\%SFw)\left(1 + \frac{P_{(w)}}{P_{(b)}}\right)$
	(Yang and Lim 2005) [22]	$\frac{\overline{\tau}_{(b)}}{\rho g h J_f} = 1 + \frac{h}{b}\frac{1}{\tan\beta} - \psi\frac{h}{b}\frac{1}{\sin\theta}$
	(Guo and Julien 2005) [23]	$\frac{\overline{\tau}_{(b)}}{\rho g h J_f} = \frac{4}{\pi}\mathrm{Arctg}\left[\exp\left(\frac{-\pi h}{b}\right)\right] + \frac{4}{\pi}\frac{h}{b}\exp\left(\frac{-h}{b}\right)$
	(Seckin, Seckin et al., 2006) [24]	$\frac{\overline{\tau}_{(b)}}{\rho g R S_f} = \frac{a + b(B/H)}{1 + c(B/H) + d(B/H)^2}$
	(Severy and Felder 2017) [25]	$\tau_0 = \frac{1}{8} f \rho V^2$
Stress intensity (K_I)	Bollaert and Schleiss 2002) [11]	$K_I = 0.8 \cdot P_{max} \cdot F \cdot \sqrt{\pi \cdot L_f}$
Lifting force (F_L)	(Bollaert and Schleiss 2002) [11]	$I = \int_0^{\Delta tpulse} (F_u - F_o - G_b - F_{sh}) \cdot dt = m \cdot V_{\Delta tpulse}$
	(Bollaert 2010) [12]	$F_{QSL} = C_{uplift} \cdot L_{block} \cdot \frac{V_{X,max}^2}{2g}$

After extensive analysis and investigation of dam construction projects, with a specific focus on hydraulic erosion within unlined spillways and its pivotal role in dam construction, the decision was taken to deeply explore this matter. Previous research concerning methodologies for assessing hydraulic erosion in dam spillways has shed light on the strengths and limitations of various approaches:

(1) Semitheoretical Approaches: Notably, Pells' RMEI method among semitheoretical approaches showcased relatively lower errors compared to counterparts within the same category, despite inherent margins of error.

(2) Semianalytical Methods: Among the array of semianalytical methods, Bollaert's CSM approach emerged as a representative choice for evaluating hydraulic erodibility, particularly in scenarios involving plunge pool dynamics. The challenges associated with obtaining site-specific data were balanced by its applicability to channel flow situations, thereby suggesting its potential as a novel analytical technique tailored for unlined spillways.

(3) Advancing Erosion Prediction Methods: The significance of developing new or refining existing erosion prediction methods was underscored as crucial for dam spillway design. This endeavor addressed the following pivotal aspects:

- Distinct Hydraulic Erosive Parameter: A foundational step involved defining a distinctive hydraulic parameter.
- Dam Spillway Geometry Influence: The influence of dam spillway geometry on the hydraulic erosive parameter.
- Impact of Rock Mass Geometry: Delving into the implications of rock mass geometry, including factors like block volume, joint characteristics, dip, and dip direction, on the hydraulic erosive parameter.
- Geomechanical Scrutiny: Definition of the effects of geomechanical factors on the hydraulic erosive parameter.

With the recognition that hydraulic erodibilty within unlined spillways encompasses both hydraulic and geomechanical aspects, this phenomenon is studied to encompass both aspects. Given the industry's reliance on established approaches like the Annandale methodology, the initial focus was directed toward the hydraulic aspect. This article stands as an important part of a comprehensive study on introducing a holistic framework

for assessing hydraulic erosion. This phase concentrated on examining the influence of geometric parameters on hydraulic parameters, setting the stage for future exploration into the interplay of geomechanical parameters with hydraulic properties. This study specifically undertook a meticulous examination of the effects of geometric parameters, with a specific emphasis on rock surface irregularities, on hydraulic parameters. The new findings provided the basis for introducing the comprehensive methodology for assessing hydraulic erodibilty. Future research phases will delve into the influence of geomechanical parameters on hydraulic parameters. Combining the knowledge accumulated from these phases will result in the development of a distinctive equation for the hydraulic erosive parameter. The ultimate objective is to present a comprehensive and coherent methodology for evaluating hydraulic erosion within unlined dam spillways.

In the article, various unlined spillway surface geometries were investigated to determine how hydraulic parameters are affected by irregularities on unlined spillway surfaces. A series of geometries found in unlined spillways were selected, and flow simulations were performed using computational fluid dynamics (CFD) with ANSYS-Fluent software. ANSYS-Fluent was chosen based on its industry-standard recognition, versatility in handling complex simulations, user-friendly interface, and robust solver options, all of which were aligned with the research requirements. These simulations were two-dimensional (2D) and were solved as steady-state flows. Within turbulent model simulations, the intricacies of irregular rock surfaces were explored—a pursuit characterized by challenges and significance. The chosen approach encompassed the utilization of the k-epsilon turbulence model with Explicit Enhanced Wall Treatment, which proficiently managed the complexities arising from surface roughness. Beyond being a necessity, the drive for accuracy assumed the role of a conduit for informed decision-making. Central to the methodology was the reliance on y+ values, serving as evaluative measures. Their impact extended to the refinement of the model and the adaptation of mesh sizes by the computed y+ values. The alterations in hydraulic parameters, including pressure (total pressure), shear stress, flow velocity, and energy, were then determined based on spillway surface geometry, i.e., irregularity height (h) and irregularity angle (α_1).

2. Materials and Methods

The flowchart of the methodology (Figure 2) presented the steps in subsections. The most effective geometric parameters of spillways and irregularities were first identified and selected by analyzing the available data from Pells [1]. Pells' data involve more than 100 case studies from dams in Australia, Africa, and the United States [1].

These selected parameters combined with observed controlled blasting patterns and available data resulted in a specific model geometry. Then, water flow over this rock geometry was simulated using ANSYS-Fluent software, and the results were extracted using CFD-Post.

The spillway geometric parameters, including spillway length and constant spillway slope, and the geometric parameters of the irregularities, including their length, height, and angle, will be explained in Section 2.1.

The purpose of this study is to provide a foundational understanding of hydraulic erosion science. This phenomenon was characterized by the synergy of hydraulic and geomechanical principles. Parameters in this science were categorized into three main groups: hydraulic, geomechanical, and geometric:

- Hydraulic parameters included total pressure, shear stress, flow velocity, force, stream power, and energy.
- Geomechanical parameters encompassed block volume, joint aperture, dip angle, and dip direction.
- Geometric parameters involved the shape of the rock surface, slope, and channel structure.

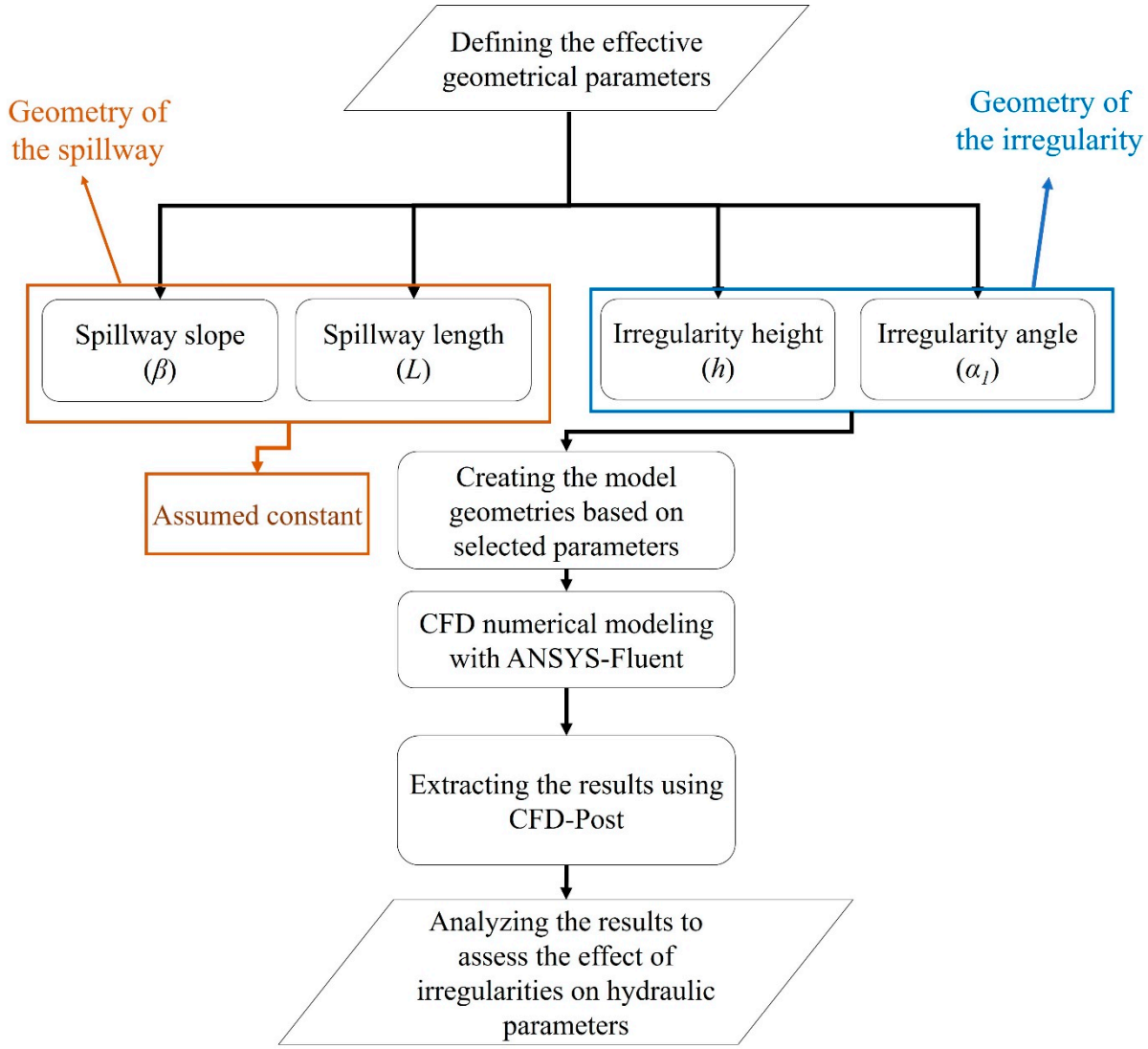

Figure 2. Flowchart presenting the steps of modeling spillway for assessing the effect of irregularity geometry on hydraulic parameters.

Given the complexity, these parameters will be analyzed separately. The focus was directed towards examining how geometric attributes, specifically the length (l), height (h), and angle (α_1) of rock surface irregularities, impacted hydraulic parameters. With the value of l held constant (given its direct relationship with other geometrical parameters), the focus was exclusively directed towards h and α_1. The investigation primarily centered on hydraulic parameters such as velocity, pressure, force, and energy. These parameters played a pivotal role, as they affected a range of other factors. By exploring the influence of h and α_1 on these hydraulic parameters, insights were gained into broader interactions.

Subsequent research delved into the impact of the remaining geometric and geomechanical factors on hydraulic parameters. Ultimately, the aspiration is to develop a comprehensive equation that integrates all attributes, offering a unified perspective on the science of hydraulic erodibility.

2.1. Determining Model Geometry

The effects of each parameter were considered separately due to the high number of variables. For this paper, only the results of irregularity height (h) and angle (α_1) are presented.

2.1.1. Step 1: Blasting Effect on the Profile of Surface Irregularities

In the context of mining, tunnelling, and dam construction, blasting is a common method of breaking and removing rock mass. In mining and tunneling operations, the high levels of detonation energy are emitted, a portion of which is productively expended on rock fragmentation [26]. Unlined dam spillways are generally built on hard rock, and controlled blasting is usually used to create the surface of the unlined spillways (Figure 3). The applied drilling and blasting produce irregularities along a spillway's surface profile [27]. When designing blasting patterns for unlined dam spillways, burden (B) and spacing (S) are important (Figure 3c). Burden denotes the distance between a blasting-hole row to the excavation face or between blasting-hole rows. Spacing refers to the distance between blasting holes along the same row [27]. According to blasting theory, the burden for hard rocks is 1–2 m. Based on the blasting patterns and the created post-blasting surfaces, the burden was considered to be equivalent to irregularity length (Figure 3d).

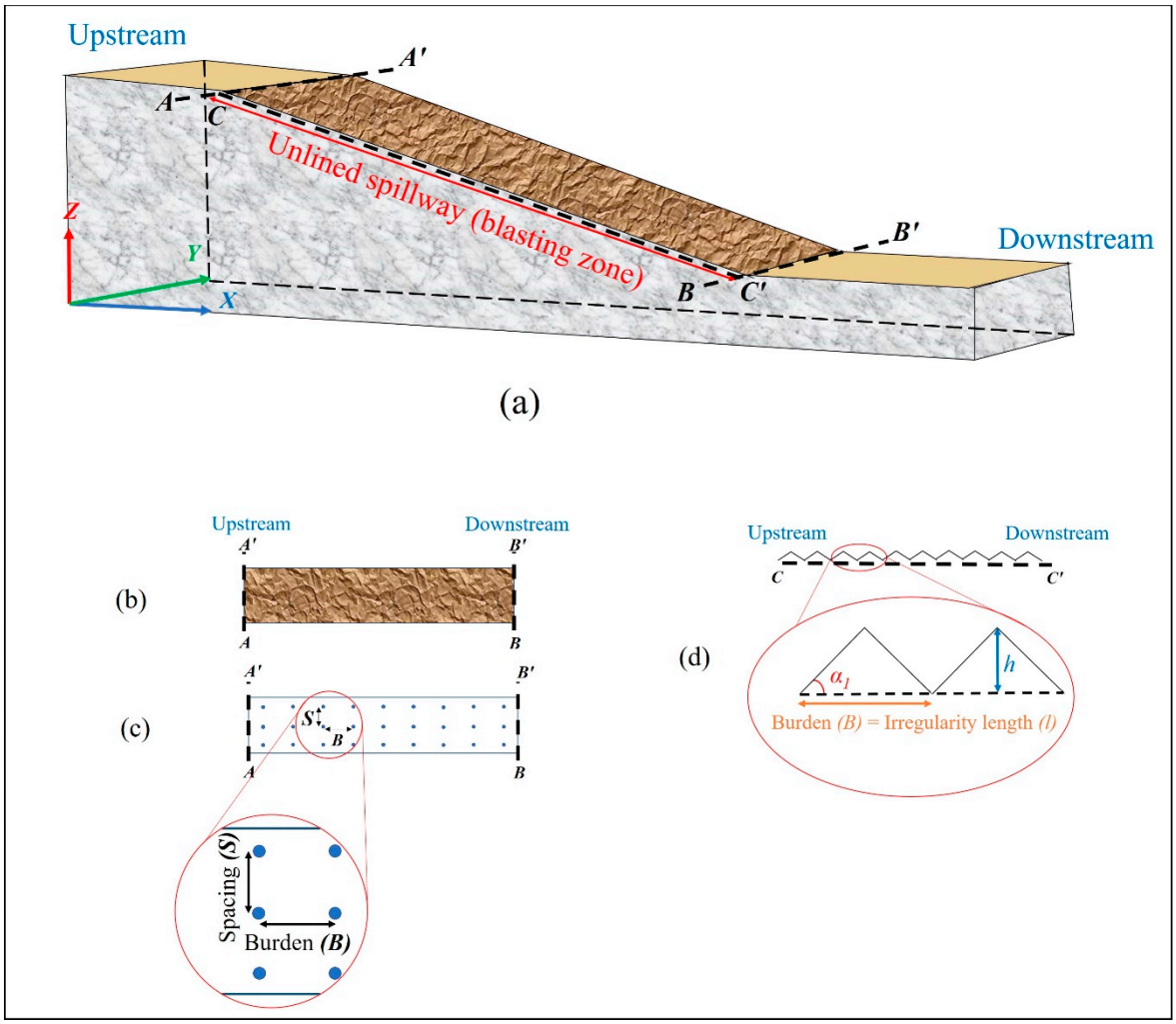

Figure 3. (**a**) Diagram of an unlined dam spillway; (**b**) channel view from above; (**c**) controlled-blasting pattern of the channel showing spacing and burden; and (**d**) channel surface profile after blasting.

2.1.2. Step 2: Selection of Geometries for Unlined Surface Profiles

In this study, the spillway geometric characteristics of spillway length (L) and spillway slope (β) were considered, and the selected geometric parameters of irregularities comprised the length (l), height (h), and angle (α_1) of the irregularities. It was assumed that the spillways' geometric parameters remained constant. An irregularity angle ranging from

12° to 40° covered most irregularities, and the irregularity height varied between 10 and 30 cm. The irregularity length was proportional to the height and angles and generally fell between 1 and 2 m. A length of 1.5 m was selected for all the models.

The geometric characteristics of the spillway (slope and length) were also considered significant, and future studies aimed to evaluate the effects of these parameters. For the models, a profile angle of 5° and a length of 50 m were selected based on observations of unlined spillways, choosing the average values of these observations (Figure 4). A total of 25 geometric configurations of spillway surface irregularities were produced.

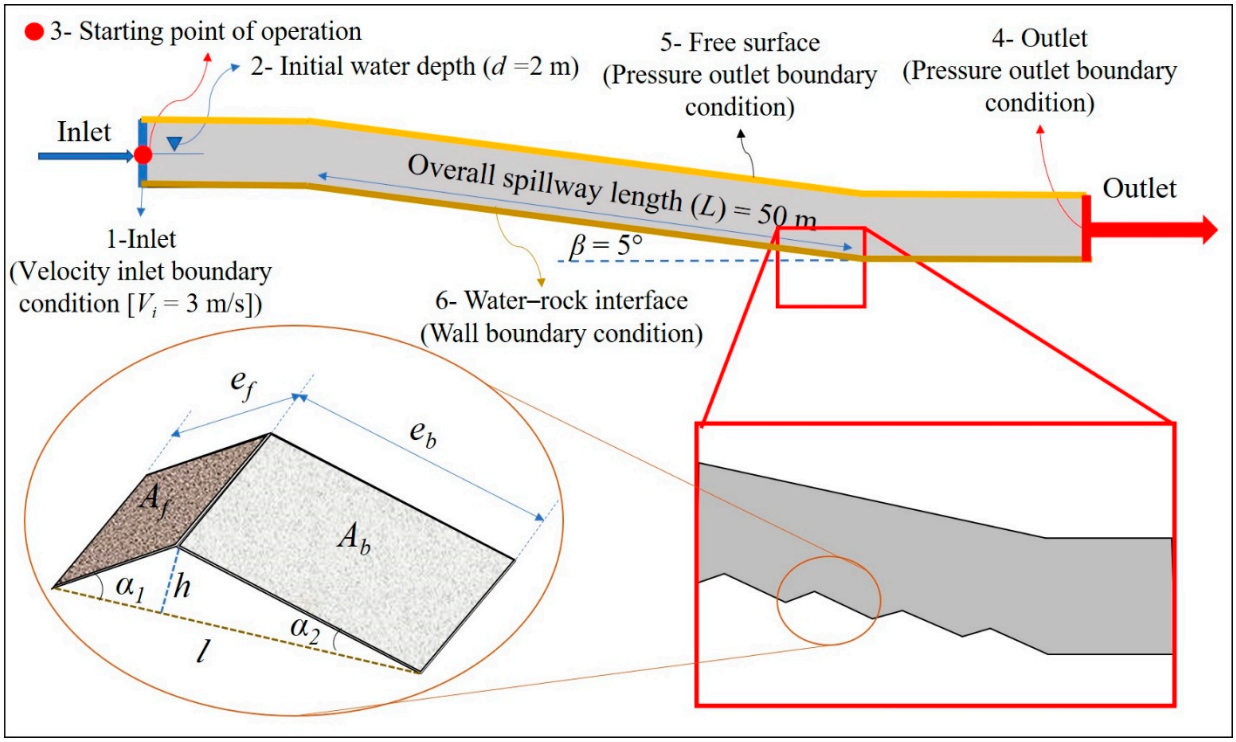

Figure 4. The assumed spillway geometry used in the model of irregularities along an unlined rock spillway.

To identify the geometric parameters of the irregularities, Equations (1)–(3) from geometry science were applied. These equations were a function of the input parameters, and the irregularity geometry could be created using these equations and the input parameters α_1, h, and l. The lengths of irregularity surfaces with and against water flow were represented by e_b and e_f, respectively (Figure 4). The irregularity angle in the flow direction, along with the spillway slope, was known as α_2. This study considered several configurations, as shown in Figure 5.

$$\alpha_2 = tan^{-1}\left(tan\,\alpha_1 \times \left(\frac{l\,tan\,\alpha_1}{l\,tan\,\alpha_1 - h} - 1\right)\right) \quad (1)$$

$$e_f = \frac{h}{sin\,\alpha_1} \quad (2)$$

$$e_b = \frac{h}{sin\,\alpha_2} \quad (3)$$

h (m) \ α_1 (°)	12	19	26	33	40
0.1	α_2 = 5.55 e_1 = 0.48 e_2 = 1.03	α_2 = 4.73 e_1 = 0.31 e_2 = 1.21	α_2 = 4.42 e_1 = 0.23 e_2 = 1.3	α_2 = 4.25 e_1 = 0.18 e_2 = 1.35	α_2 = 4.14 e_1 = 0.16 e_2 = 1.38
0.15	α_2 = 10.7 e_1 = 0.72 e_2 = 0.81	α_2 = 8.02 e_1 = 0.46 e_2 = 1.07	α_2 = 7.17 e_1 = 0.34 e_2 = 1.2	α_2 = 6.74 e_1 = 0.28 e_2 = 1.28	α_2 = 6.48 e_1 = 0.23 e_2 = 1.33
0.2	α_2 = 19.7 e_1 = 0.96 e_2 = 0.59	α_2 = 12.28 e_1 = 0.61 e_2 = 0.94	α_2 = 10.4 e_1 = 0.46 e_2 = 1.11	α_2 = 9.52 e_1 = 0.37 e_2 = 1.21	α_2 = 9.01 e_1 = 0.31 e_2 = 1.28
0.25	α_2 = 37.7 e_1 = 1.2 e_2 = 0.41	α_2 = 17.9 e_1 = 0.77 e_2 = 0.81	α_2 = 14.21 e_1 = 0.57 e_2 = 1.02	α_2 = 12.64 e_1 = 0.46 e_2 = 1.14	α_2 = 11.75 e_1 = 0.39 e_2 = 1.23
0.3	α_2 = 73.54 e_1 = 1.44 e_2 = 0.31	α_2 = 25.5 e_1 = 0.92 e_2 = 0.7	α_2 = 18.73 e_1 = 0.68 e_2 = 0.93	α_2 = 16.12 e_1 = 0.55 e_2 = 1.08	α_2 = 14.71 e_1 = 0.47 e_2 = 1.18

Figure 5. Configurations of the various modeled spillway surface irregularities.

2.2. Numerical Modeling

To simplify the computation of wall parameters on irregular surfaces, ANSYS-Fluent Version 2020 R2 was used in this study. ANSYS-Fluent converts scalar transport equations into algebraic equations that can be run numerically on the basis of a controlled volume approach. Functioning within a 2D framework, the CFD model was employed to solve under steady-state conditions. This configuration allowed for a focused examination of essential fluid dynamics aspects. The objective behind these simulations was to capture the sensitivity of hydraulic parameters to irregularities present on the rock surface. The open-channel submodel in ANSYS-Fluent, partially based on the volume of fluid (VOF) multiphase model, was used in the analysis [28]. In the original VOF technique, Hirt and Nichols [29] used a specialized methodology to obtain a standard definition of the free surface, whereas ANSYS-Fluent solves the combined air–water flow systems [30]. In the realm of turbulent model simulations, the investigation of irregular rock surfaces emerges as both a challenge and an avenue of significance. The selected path involves employing the k-epsilon turbulence model with Enhanced Wall Treatment, a strategic choice well-suited for addressing the intricacies arising from surface roughness. This approach, motivated by the pursuit of accuracy as a foundation for informed decision-making, hinges on the pivotal role of y+ values. Y+ values, acting as evaluative indicators, play a crucial role in refining the model and adjusting mesh sizes. Serving as a touchstone for near-wall resolution in turbulent simulations, y+ values enable the calibration of the model's mesh. This calibration, guided by the computed y+ values, fine tunes the mesh sizes, ensuring a harmonious fit that mirrors real-world intricacies accurately. Within the framework of k-epsilon turbulence modeling, precise alignment with y+ values not only rectifies errors arising from improper meshing but also creates a simulation environment faithfully capturing the physics near rough wall interfaces. Incorporating the y+ value and executing grid convergence analysis on several parameters, endeavors were made to confine them within the range of $1 < y+ < 30$. Following successive iterations of mesh refinement and subsequent reduction, the y+ value was progressively brought to an approximate range of 30. The accuracy of the model was subsequently evaluated through rigorous grid convergence analysis, closely associated with the y+ values.

Solutions to the Navier–Stokes equations were derived using a stable, implicit technique in the simulations. Pressure–velocity coupling was treated for stability using the widely used COUPLED method. To enhance momentum, a second-order upwind scheme was applied in this study.

Table 2 presented the model input data for the fluid flow modeling. A 3 m/s velocity-inlet boundary condition was applied. In open channels, upstream velocity–inlet boundary conditions define the flow velocity and relevant scalar characteristics of the flow at the flow inlet. At the outflow zone, a pressure–outlet boundary condition was specified.

A no-slip boundary condition was assumed at the water–rock interface (Figure 4). The water depth at the model's entrance (inlet) was the starting point for the simulation calculations. Atmospheric pressure and a 2 m water depth were also set in the model. Figure 6 shows the produced model in ANSYS-Fluent and the meshing used. To avoid the impact of localized bursts, it was effectively mitigated by the employed mesh refinement strategy, thereby enhancing the fidelity of CFD simulations. The ultimate aim was to attain an optimum simulation model that harmonized accuracy and cost-effectiveness.

Table 2. Input parameters used in the computational fluid dynamics (CFD) modeling.

Parameters	Value	Description
Initial flow depth	2 m	See point 3 in Figure 4
Initial flow velocity	3 m·s^{-1}	See point 1 in Figure 4
Inlet boundary condition	–	Velocity inlet (point 1 in Figure 4)
Outlet boundary condition	–	Pressure outlet (point 4 in Figure 4)
Unlined spillway length	50 m	–
No. of irregularities	32	–
Irregularity height (h)	10, 15, 20, 25, 30 cm	
Irregularity angle (α_1)	12°, 19°, 26°, 33°, 40°	
Channel slope	5°	–

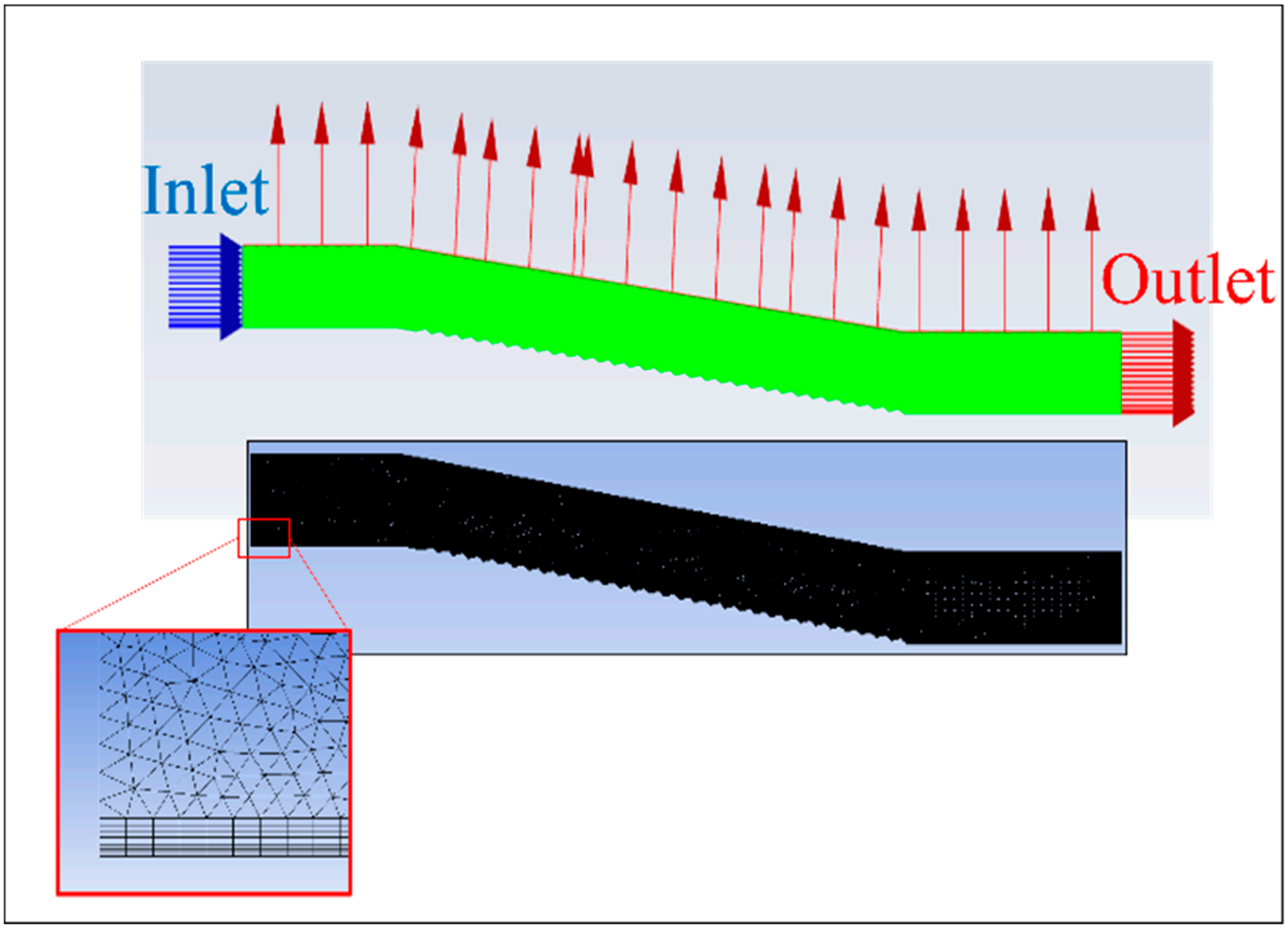

Figure 6. Diagram of the numerical modeling and the applied meshing.

2.2.1. Step 1: Model Geometry and Boundary Conditions

Designing the geometry is the first step of *CFD* numerical modeling. Therefore, various simulation geometries were produced using the ANSYS geometry tool. Five irregularity heights (h) and five irregularity angles (α_1) were identified based on the Pells data set. A total of 25 configurations were considered for this study (Figure 5).

2.2.2. Step 2: Meshing and Convergence Analysis

In the research, the physical model was mesh-constructed using a triangular structural grid. An inflation layer was applied along the spillway wall, and the mesh gradually increased in size from bottom to top to provide a more accurate simulation that captured the boundary layer. At the channel bottom, five inflation layers with a growth rate of 1.2% were considered.

To determine whether the precision of the numerical simulations was affected by grid cell size—and to find the optimal grid size—the first branch–channel physical model was meshed using five distinct techniques (the maximum grid cells were 20, 15, 10, 5, and 1 cm). This analysis was conducted for the final irregularity along the spillway, and the results were evaluated in terms of total pressure, maximum velocity, and water depth for h = 10 cm and $\alpha_1 = 12^\circ$. A meshing size of 10 cm was deemed optimal on the basis of outcomes of this grid convergence analysis (Table 3), considering the criteria of the time calculation and precision of the results. Finally, an approximately 48 m long portion of the channel (CC′ red line in Figure 3a) was analyzed.

Table 3. Grid independence study at the last irregularity.

Boundary Conditions	**Structural Schemes**				
Maximum size of grid cell (cm)	20	15	10	5	1
Maximum velocity ($m \cdot s^{-1}$)	9.46	10.31	10.64	10.68	10.67
Water depth (cm)	82.1	73.3	68.9	68.1	67.9
Maximum total pressure (kPa)	52.63	60.16	63.18	63.52	63.6

2.2.3. Step 3: Model Setup (VOF Method, Turbulence Model, Control Equation)

Free surface channel fluctuations impact both the air and water phases and complicate the modeling. By resolving a single momentum equation and storing a record of the volume fraction of each immiscible fluid inside the computational region, the VOF model can simulate two or more immiscible fluids. Moreover, the VOF approach can be applied to a wide range of discontinuous interfaces and flowing water and allows monitoring the water surface in open channels. The sum of all volume fractions of all phases in each control body is one [31].

$$a_w + a_a = 1 \tag{4}$$

where a_w and a_a represent the volume fractions of water and air, respectively. When a_w = 1, water fills every control unit in the calculation domain, and when a_a = 1, it fills with air. Tracking the air–water interaction requires the following continuity equation [32]:

$$\frac{\partial a_w}{\partial a_a} + u_i \frac{\partial a_w}{\partial x_i} = 0 \tag{5}$$

where X_i represents the coordinate and u_i denotes the flow velocity. (For units of the various parameters, please refer to the included symbol notation table)

Both the continuity and momentum equations for a free and incompressible fluid in an open channel can be expressed as

$$\frac{\partial u}{\partial x} + \frac{\partial v}{\partial y} = 0 \tag{6}$$

$$\rho\frac{\partial u}{\partial t} + \rho\ \mathrm{div}(uV) = \mu\ \mathrm{div}(\mathrm{grad}\ u) - \frac{\partial P}{\partial x} + F_u, \text{ and} \tag{7}$$

$$\rho\frac{\partial v}{\partial t} + \rho\ \mathrm{div}(vV) = \mu\ \mathrm{div}(\mathrm{grad}\ v) - \frac{\partial P}{\partial y} + F_v \tag{8}$$

where V is the flow velocity, u and v are the velocity components of fluid particles in the 2D spatial directions x and y, ρ is the density of water, μ is the dynamic viscosity, P is the pressure (P_a), and F_u and F_v are the forces of fluid particles in 2D directions.

The RNG k-ϵ turbulence model eliminates average flow rotation and whirling by modifying turbulent viscosity. The related equation is [33]

$$\frac{\partial(\rho k)}{\partial t} + \frac{\partial(\rho k u_i)}{\partial x_i} = \frac{\partial}{\partial x_i}\left[\alpha_k \mu_{eff}\frac{\partial k}{\partial x_j}\right] + G_k + \rho\epsilon \tag{9}$$

$$\frac{\partial(\rho\epsilon)}{\partial t} + \frac{\partial(\rho\epsilon u_i)}{\partial x_i} = \frac{\partial}{\partial x_i}\left[\alpha_\epsilon \mu_{eff}\frac{\partial \epsilon}{\partial x_j}\right] + \frac{C_{1\epsilon}}{k}G_k - C_{2\epsilon}\rho\frac{\epsilon^2}{k}, \text{ and} \tag{10}$$

$$G_k = \mu_t\left(\frac{\partial u_i}{\partial x_j} + \frac{\partial u_j}{\partial x_i}\right)\frac{\partial u_i}{\partial x_j} \tag{11}$$

where k denotes the turbulent kinetic energy, ϵ represents the turbulent energy dissipation rate, μ expresses the hydrodynamic viscosity coefficient, G_k denotes the turbulent kinetic energy production term, μ_{eff} represents the effective dynamic viscosity coefficient $C_{1\epsilon}$ and $C_{2\epsilon}$ denote the constants 1.42 and 1.68, respectively.

3. Results

The effect of surface irregularity on pressure, stress, flow velocity, and energy were evaluated under 25 different irregularity configurations. In the following subsections, the effects of irregularities on the hydraulic parameters are examined independently. Figure 7 shows the software output, depicting the volume fraction of water (*VF*), the contours of dynamic pressure (P_D) and total pressure (P_T) extracted directly from Ansys_Fluent.

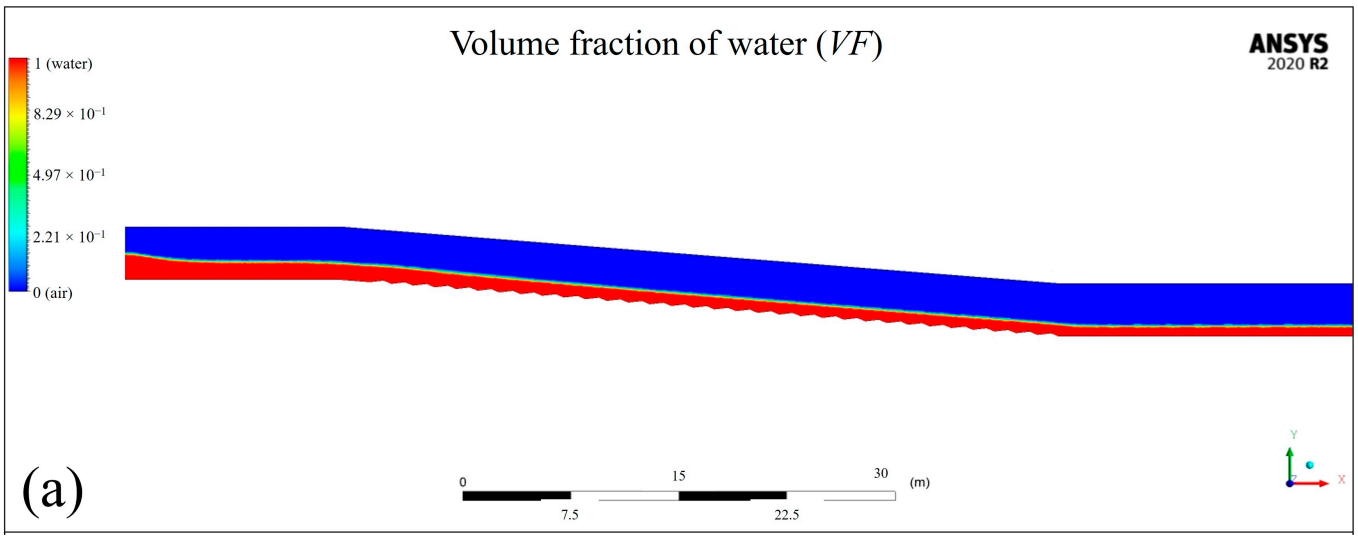

Figure 7. *Cont.*

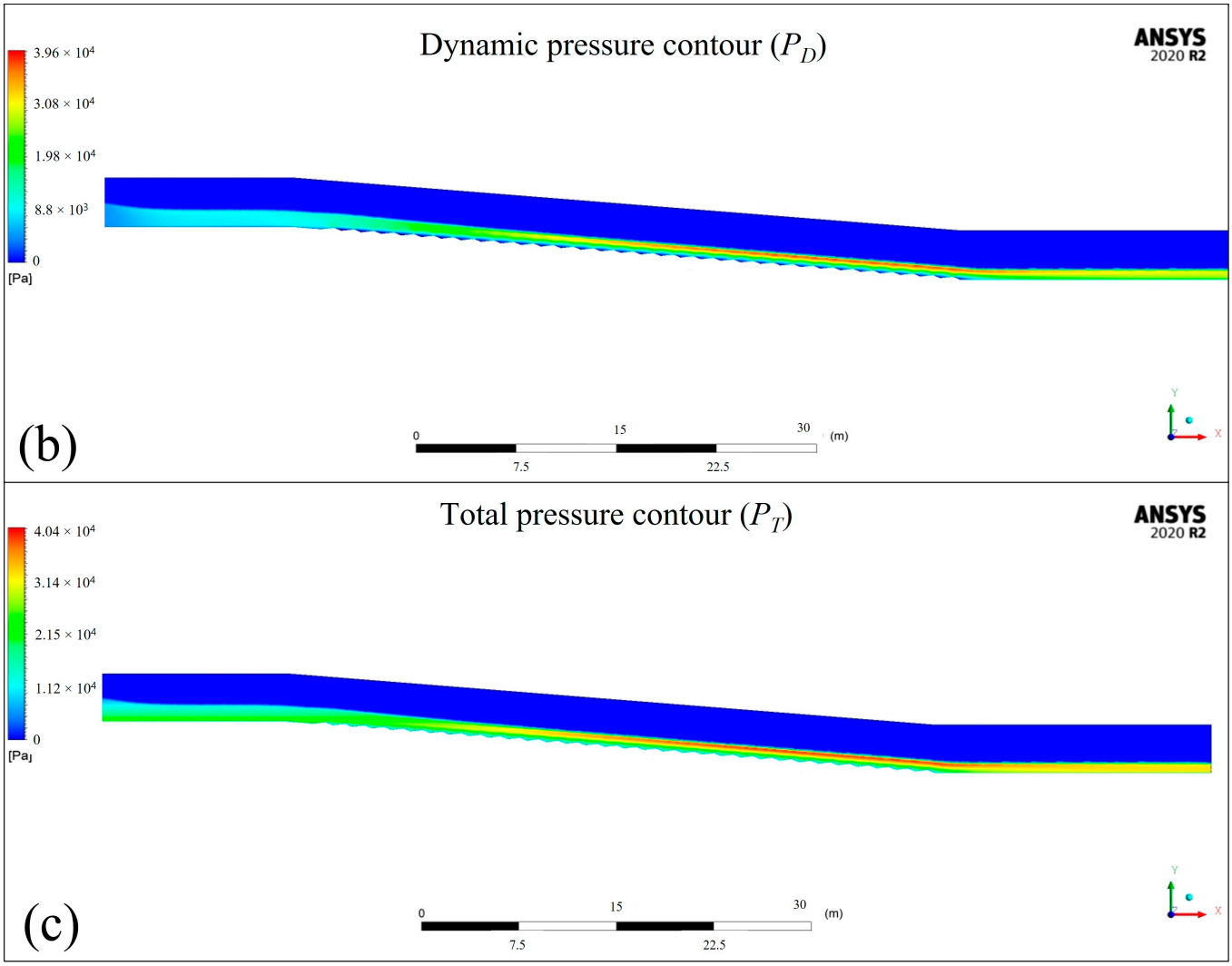

Figure 7. (**a**) The contour of volume fraction of water, (**b**) dynamic pressure contour, and (**c**) total pressure contour.

3.1. Effect of Irregularities on Velocity

Eleven vertical cross-sections were analyzed along the spillway to estimate the maximum velocity profile. Each section covered the channel bottom to the water's surface, allowing us to calculate maximum velocity and water depth. Along the spillway, maximum velocity decreased as α_1 and height increased (Figure 8). Moreover, the effect of height on flow velocity was greater than the effect of α_1. For instance, at a constant α_1 (α_1 = 12), maximum velocity decreased from approx. 11.5 m·s^{-1} at h = 10 cm to approx. 8 m·s^{-1} at h = 40 cm. At a constant height, however, velocity did not necessarily decrease as α_1 increased, the change often being minor and could be ignored. For instance, at a constant height (h = 10 cm), the maximum velocity for α_1 = 12 was approx. 11.5 m·s^{-1} and for α_1 = 40, it was approx. 9 m·s^{-1}. Flow velocity did not change significantly at a constant height (i.e, h = 30 cm) as α_1 increased. At greater heights (h), α_1 variations did not affect maximum velocity, and the height of the irregularity had a greater impact.

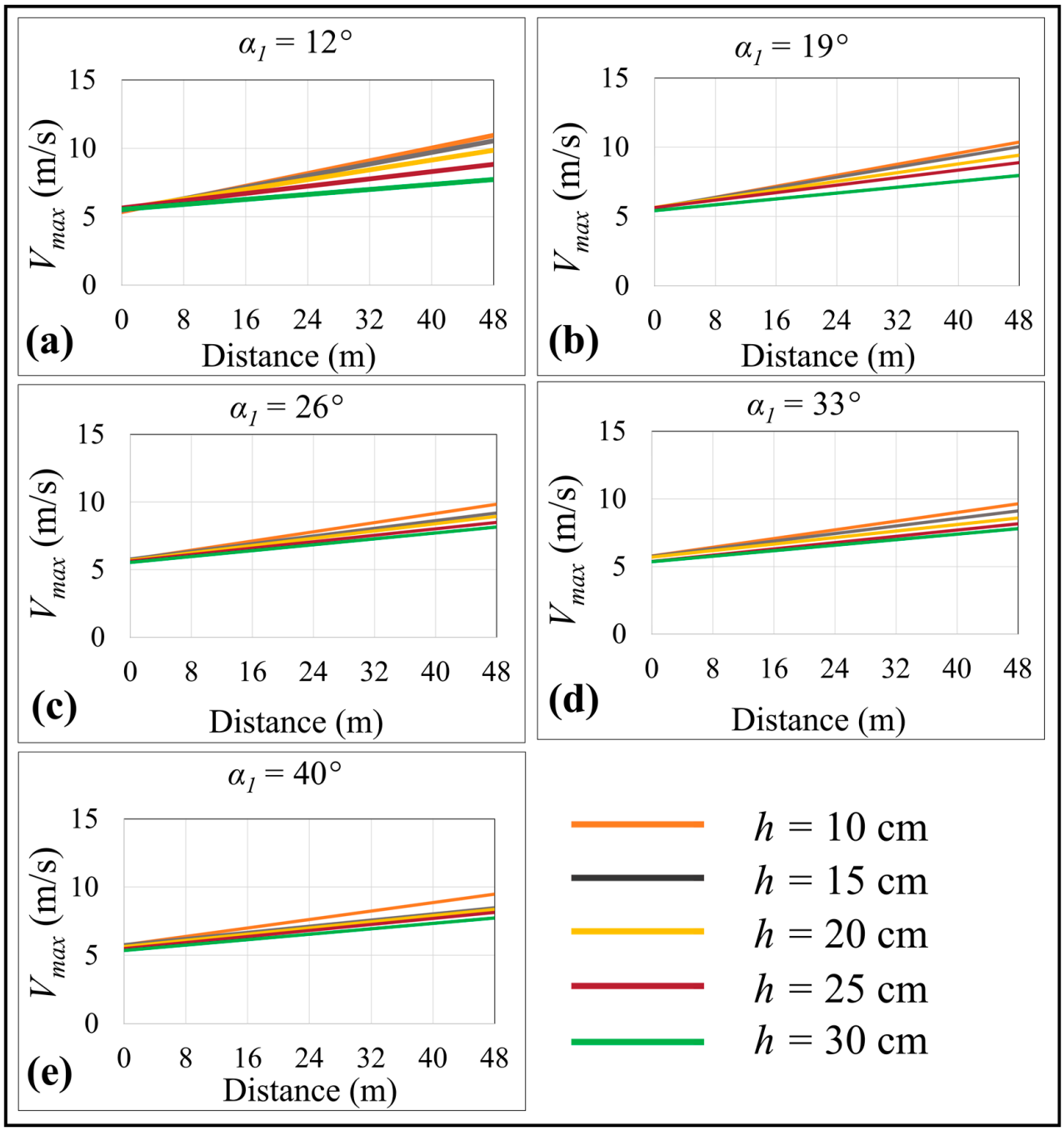

Figure 8. Maximum velocity profiles of the flow along the unlined spillway; (**a**) $\alpha_1 = 12°$; (**b**) $\alpha_1 = 19°$; (**c**) $\alpha_1 = 26°$; (**d**) $\alpha_1 = 33°$; (**e**) $\alpha_1 = 40°$.

When velocity was evaluated as a function of flow depth at various irregularity heights (for the final irregularity along the channel), it was observed that a greater irregularity height, at a constant irregularity angle, caused water depth to increase, and the maximum velocity was also higher (Figure 9).

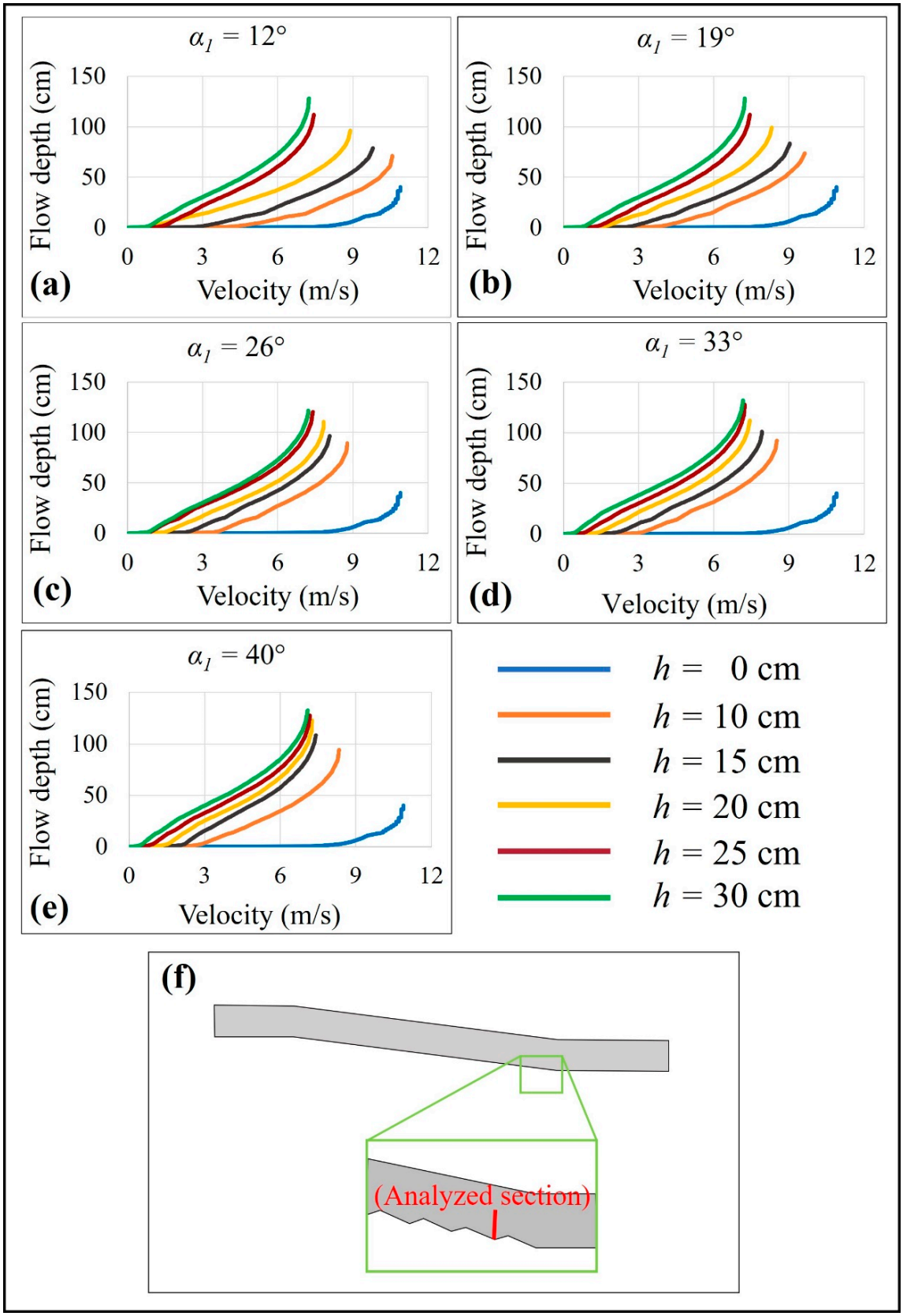

Figure 9. Velocity profiles as a function of flow depth for various irregularity heights; a flow depth of 0 m refers to the channel bottom; (**a**) α_1 = 12°; (**b**) α_1 = 19°; (**c**) α_1 = 26°; (**d**) α_1 = 33°; (**e**) α_1 = 40°; (**f**) the analyzed section of the channel profile (red line).

3.2. Effect of Irregularities on Total Pressure (P_T)

In hydraulic engineering, total pressure is the sum of static and dynamic pressures. The relationship between total, static (P_S), and dynamic (P_D) pressures are described in Equations (12)–(14), respectively.

$$P_T = P_S + P_D \tag{12}$$

$$P_S = \rho g d, \text{ and} \tag{13}$$

$$P_D = \frac{1}{2}\rho v^2 \tag{14}$$

where ρ is the density of water, g is the gravitational acceleration, d is the water depth, and v is the local flow velocity.

Total pressure in the first section was derived directly from the ANSYS-Fluent results, which produced a total pressure profile at the water–rock interface (channel bottom). When static pressure was at its maximum, dynamic pressure was at its minimum (Equation (15)).

When calculating the total pressure, both the maximum static and maximum dynamic pressure were considered (Equation (16)).

$$P_T = P_{S,channel\ bottom} + P_{D,channel\ bottom} \text{ and} \tag{15}$$

$$P_{T,max} = P_{S,channel\ bottom} + P_{D,water\ surface} \tag{16}$$

where $P_{T,max}$ represents maximum total pressure, $P_{S,channel\ bottom}$ represents the static pressure at the channel bottom, $P_{D,channel\ bottom}$ represents the dynamic pressure at the channel bottom, and $P_{D,water\ surface}$ is the dynamic pressure at the water surface, where it is at its maximum.

At the bottom of the channel, total pressure fluctuated along the spillway length (Figure 10, for h = 10 cm and α_1 = 19°). To analyze these fluctuations, the most representative and appropriate lines, which represented the upper bound of each graph (e.g., red line of Figure 10), for each configuration were selected. These lines were then grouped into a single chart (Figure 11).

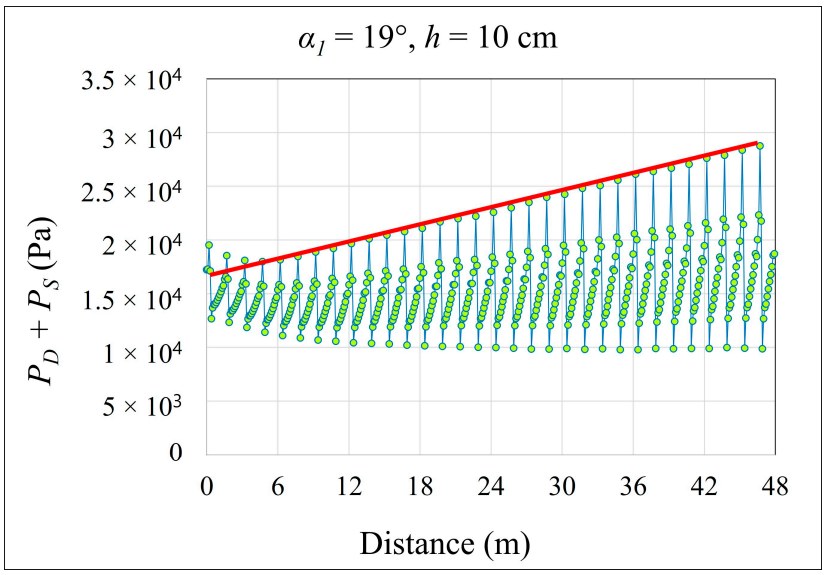

Figure 10. Total pressure (sum of dynamic and static pressures) profile along the water–rock interface for the configuration α_1 = 19° and h = 10 cm; red line describes the upper bound of the graph.

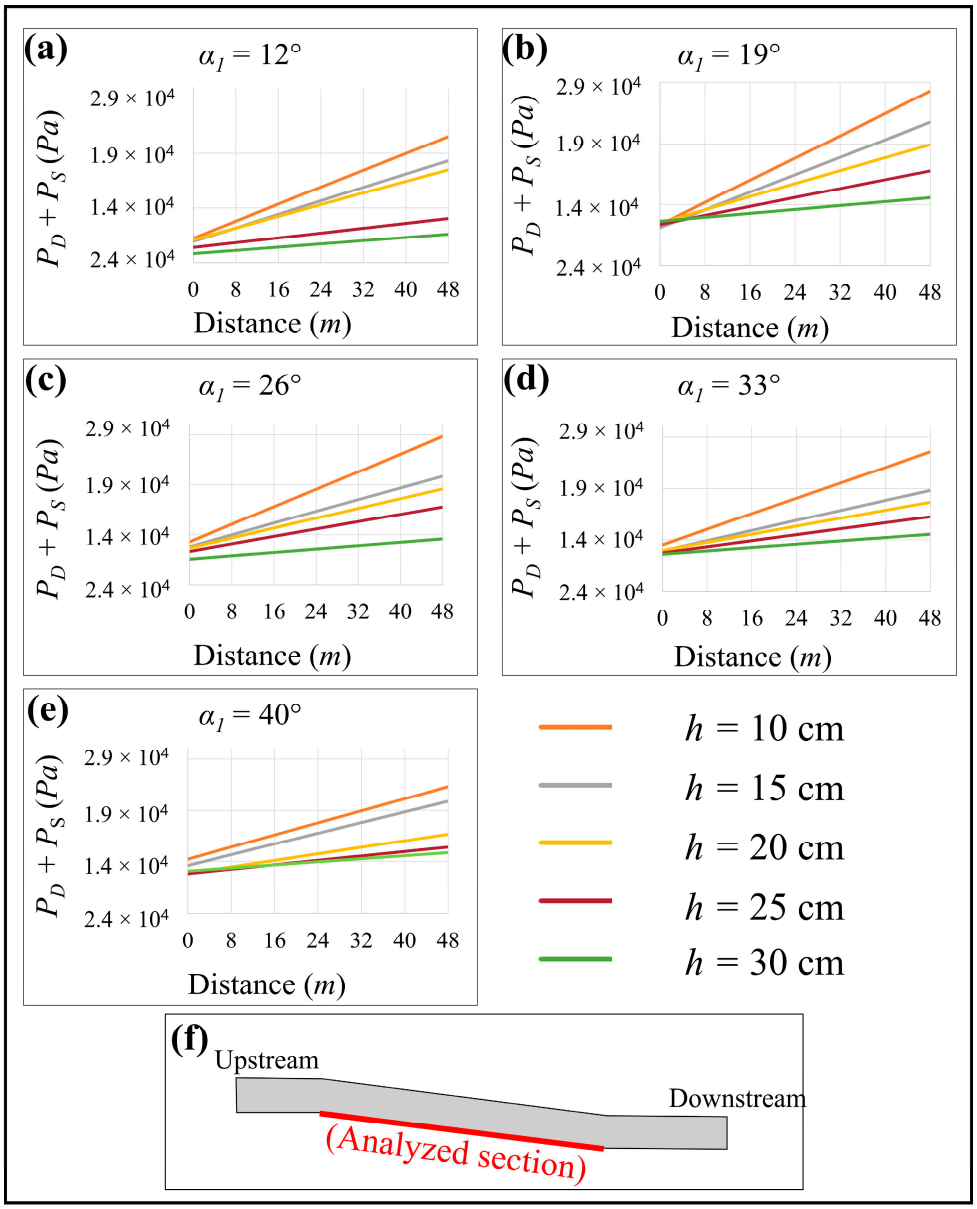

Figure 11. Total pressure (static and dynamic pressure) profiles on water–rock interface as a function of spillway length for various irregularity heights and angles; (**a**) $\alpha_1 = 12°$; (**b**) $\alpha_1 = 19°$; (**c**) $\alpha_1 = 26°$; (**d**) $\alpha_1 = 33°$; and (**e**) $\alpha_1 = 40°$; (**f**) the analyzed section of the channel profile (red line).

Flow velocity increased, and water depth decreased moving downstream; thus, dynamic pressure, which has a direct relationship with flow velocity, trended upward, whereas static pressure, which has a direct relationship with water depth, trended downward along the channel. Overall, total pressure increased toward the downstream end of the profile. According to hydraulic engineering theory, however, flow velocity at the channel bottom is zero; thus, the dynamic pressure should also be zero. Total pressure at the channel bottom should be a function of static pressure, which also trends downward along the profile. The apparent contradiction of an increasing total pressure along the channel bottom and the greater role of dynamic pressure arose as the ANSYS-Fluent software records dynamic pressures at the mesh cell center. The value shown along the wall appears to be an extrapolation that does not necessarily equal zero.

It was observed that total pressure decreased as α_1 and h increased (Figure 11). For example, at a constant $\alpha_1 = 12°$, the total pressure of flowing water at the channel bottom

dropped with a higher h, from approx. 25 Pa at h = 10 cm to approx. 17 Pa at h = 40 cm. At a constant h, however, total pressure did not necessarily decrease as α_1 increased; often these changes were negligible and could be ignored. At greater heights (h), altering α_1 produced little effect on total pressure, whereas altering the height of the irregularity had a marked effect. The total pressure difference at the zero point occurred because the zero point on the X-axis (distance) did not match the model's zero point (see Figure 11f). The analysis began 15 m from the model's inlet; thus, the effect of irregularity height could already be observed, causing the initial pressure difference in the graphs.

The total pressure was calculated using Equation (16). Since dynamic pressure is determined using the maximum velocity, the total pressure reached its maximum at the highest velocities (Figure 12). Consequently, both dynamic and static pressures along the channel bottom were also at their maximum. Additionally, it was observed that the total pressure increased by 2.5–3 times compared to the pressure along the channel bottom. Total pressure also decreased as α_1 and h increased (Figure 12). At greater heights (h), α_1 changes had minimal effect on the total pressure, whereas changes to irregularity height did produce a large effect.

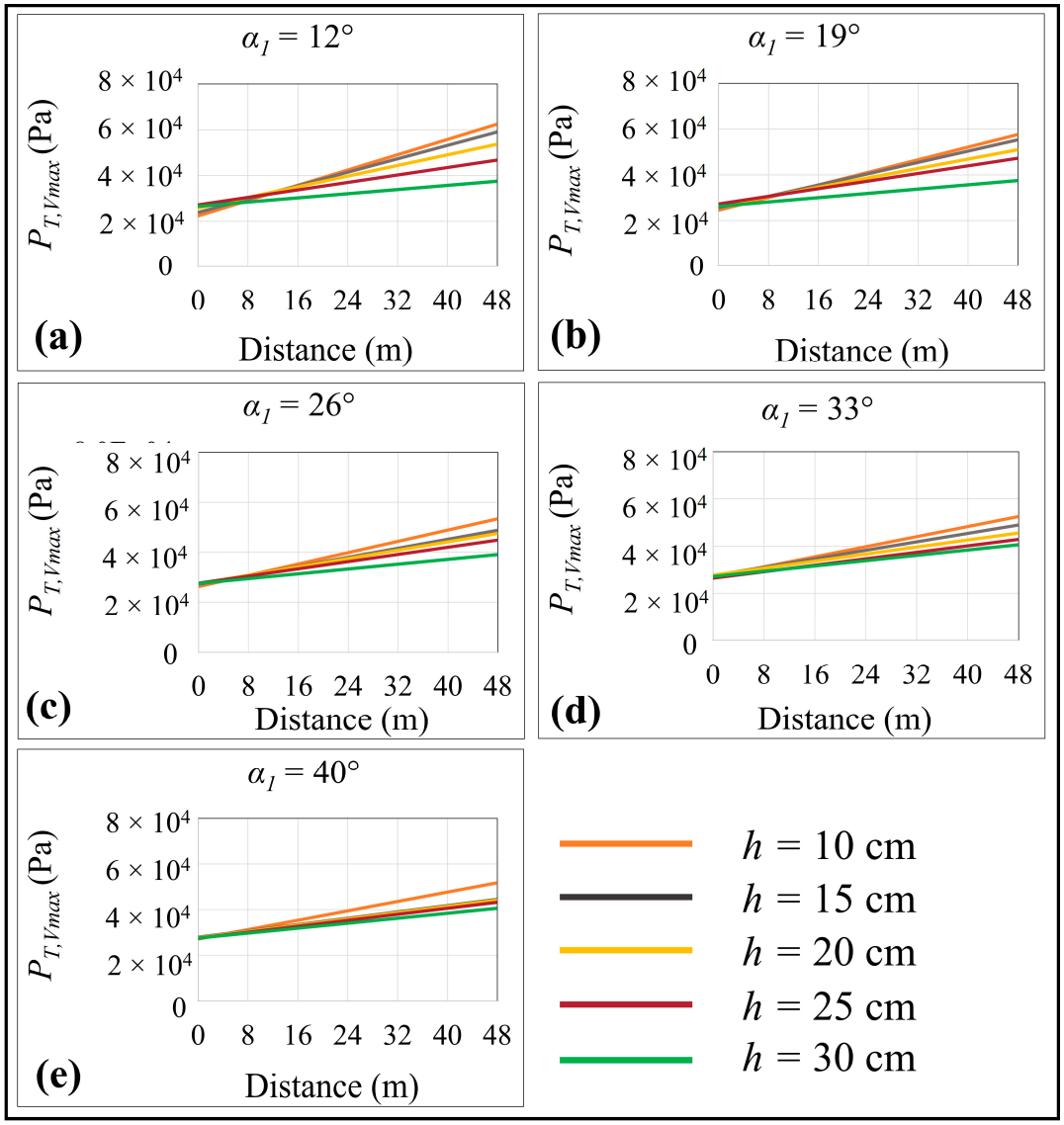

Figure 12. Total pressure profiles on the water surface as a function of spillway length for various irregularity heights; (**a**) α_1 = 12°; (**b**) α_1 = 19°; (**c**) α_1 = 26°; (**d**) α_1 = 33°; and (**e**) α_1 = 40°.

3.3. Effect of Irregularities on Shear Stress

Shear stress at the water–rock interface was also investigated. Figure 13 shows the surface shear stress on the rock surface for an irregularity angle of α_1 = 12. Shear stress on the rock surface was negligible relative to the total, static, and dynamic pressures. Nonetheless, as irregularity height (h) increased, shear stress along the wall decreased; however, these values were so small that they could be ignored.

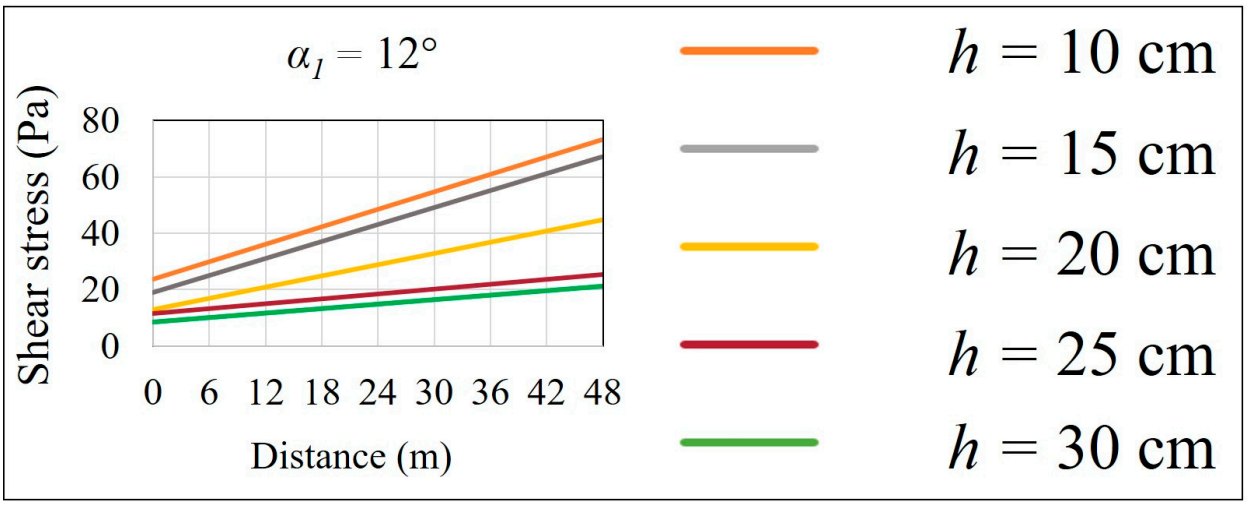

Figure 13. Shear stress along the water–rock interface for an irregularity angle of $\alpha_1 = 12°$.

3.4. Effect of Irregularities on the Energy Gradient

In the preceding section, the sum of pressure and velocity heads, i.e., dynamic and static pressure, for two distinct states of dynamic pressure, namely (1) at the rock mass surface and (2) at the water surface, was described. Here, the energy at (1) the water surface and (2) the channel bottom was analyzed.

The relevant energy was computed using Equations (17) and (18), with velocity head determined directly from the flow velocity, and pressure head equal to water depth. The elevation of a point was its distance from the datum.

$$E_{\text{water}-\text{rock interface}} = H_{P,WRI} + H_{V,WRI} + Z_{WRI}, \text{ and} \quad (17)$$

$$E_{water\ surface} = H_{P,W.S} + H_{V,W.S} + Z_{W.S} \quad (18)$$

where $E_{\text{water}-\text{rock interface}}$ represents the energy at the channel bottom, $H_{P,\ WRI}$ and $H_{V,\ WRI}$ are the pressure head and velocity head, respectively, at the channel bottom. $Z_{\ WRI}$ is the elevation of the channel bottom, $E_{Water\ surface}$ is the energy at the water surface, $H_{P,\ WS}$ and $H_{V,\ WS}$ represent, respectively, the pressure head and velocity head at the water surface, $Z_{\ WS}$ is the elevation of the water surface from the datum, and $Z_{\ water\ surface} = Z_{\ rock} + H_{P,\ WRI}$. These parameters are mesured in meters.

For calculating the energy at the rock mass surface, the velocity head was at a minimum and the pressure head at a maximum. In contrast, at the water surface, the velocity head was at a maximum, and the pressure head was zero. The difference between the energy at the water surface and the energy at the channel bottom ($E_{\text{water}-\text{rock interface}}$) was the velocity head or dynamic pressure. Figure 14 describes the methodology to calculate energy at the water–rock interface and water surface.

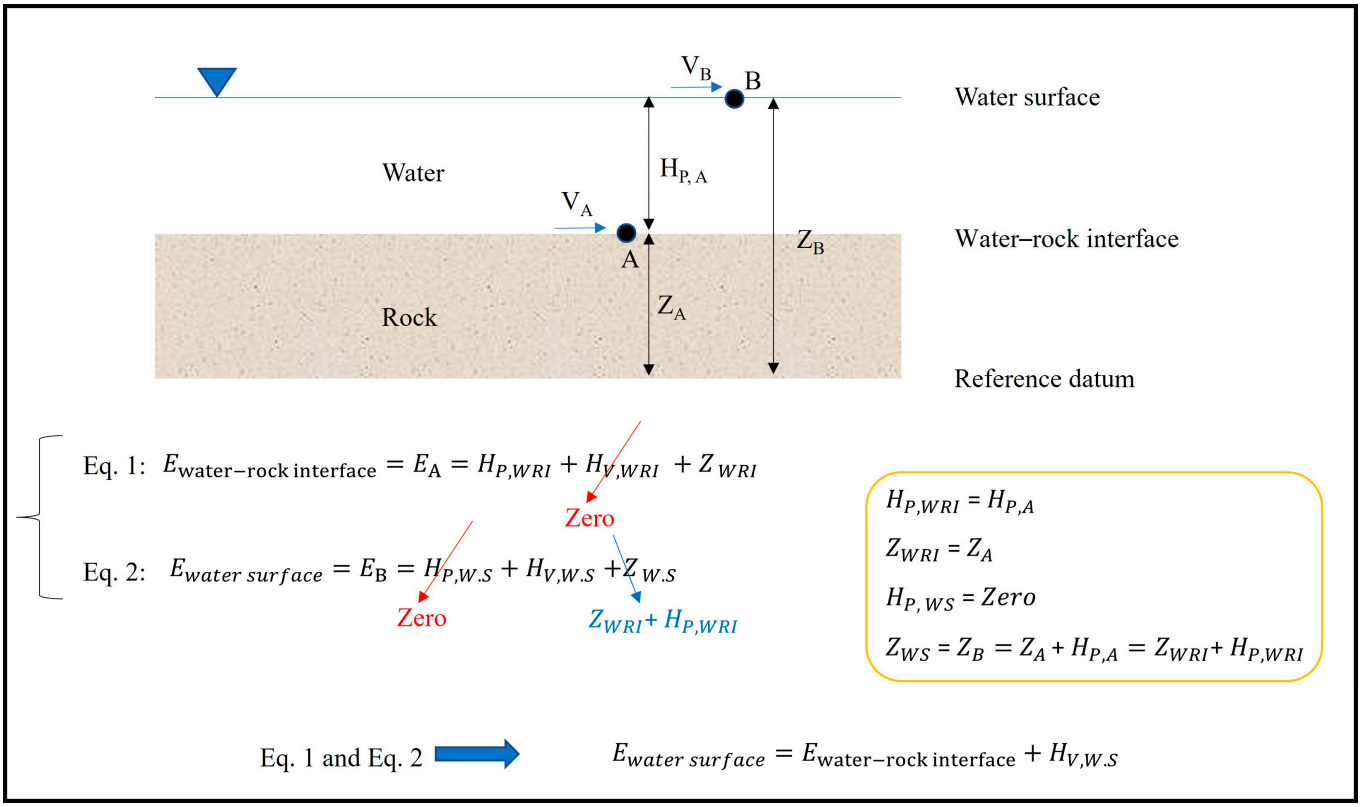

Figure 14. Calculation of energy at the water–rock interface and water surface.

The energy of water at the water–rock interface and water surface for the entire analyzed area was then calculated. Energy gradients and differences in energy along the profile were also depicted (Figure 15). Energy decreased upstream to downstream, with 70% of the energy lost along the profile. When the angle was held constant, as h increased, a greater amount of energy was lost. Less energy was lost when h decreased. At a constant h, however, energy loss was not necessarily greater as α_1 increased.

Energy at the water surface (State 1) where energy relates to elevation and velocity head (at their maximum) and the pressure head are at their minimum. Energy increased along the profile relative to the energy at the water–rock interface (State 2). This energy increase was around 30% upstream and 2.5–3.5× times downstream relative to the energy at water–rock interface.

Differences in the energy state at the water–rock interface (Figure 15) and the water surface (Figure 16) related to the flow velocity and dynamic pressure.

Energy loss at the water–rock interface (State 1) was greater than at the water surface (State 2) because:

- In the first state, the velocity differential between upstream and downstream was close to zero; thus, the slope of the flow–distance relationship was zero;
- In the second state, the difference in velocity between the upstream and downstream was not zero, and flow velocity–distance relationship sloped upward.

Because the sum of Z and H_P was the same for both states, the negative relationship between the energy and distance decreased as the slope of the velocity increased for the second state, i.e., a greater velocity increased the amount of energy and decreased energy loss.

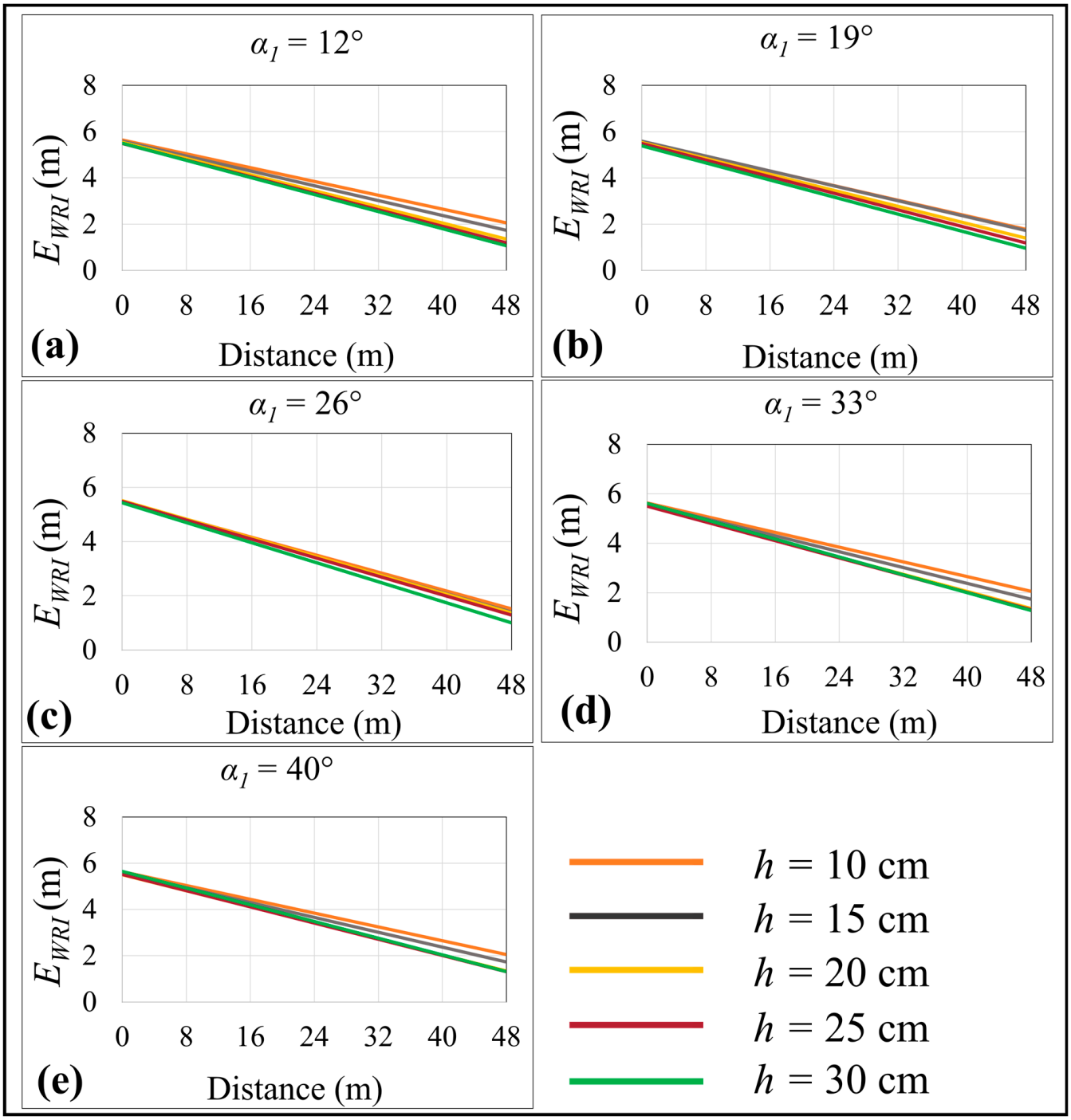

Figure 15. Energy gradient profiles at the water–rock interface; (**a**) $\alpha_1 = 12°$; (**b**) $\alpha_1 = 19°$; (**c**) $\alpha_1 = 26°$; (**d**) $\alpha_1 = 33°$; and (**e**) $\alpha_1 = 40°$.

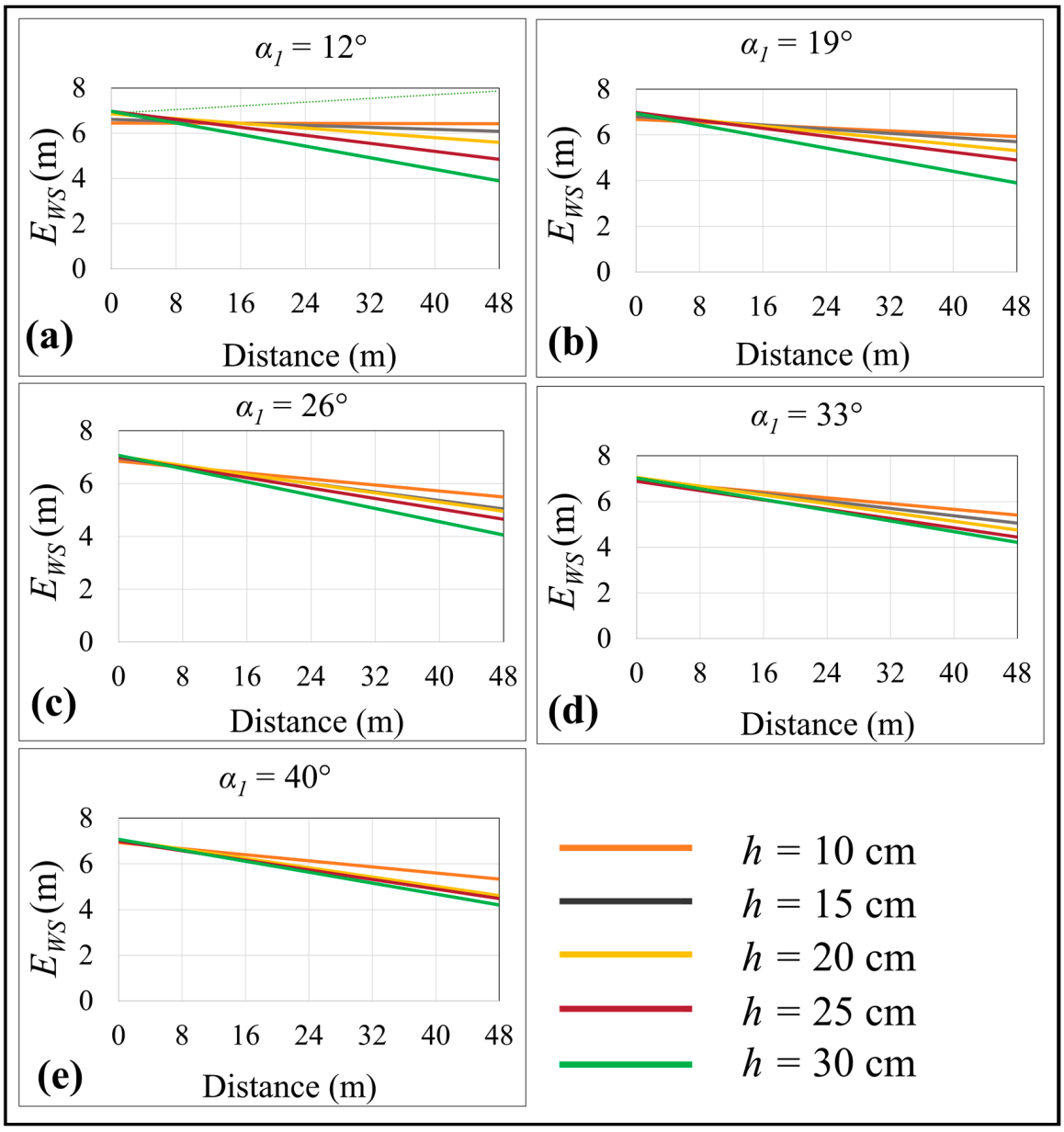

Figure 16. Energy gradient profiles along the water surface; (**a**) $\alpha_1 = 12°$; (**b**) $\alpha_1 = 19°$; (**c**) $\alpha_1 = 26°$; (**d**) $\alpha_1 = 33°$; and (**e**) $\alpha_1 = 40°$.

4. Discussion

Our study demonstrated the successful use of ANSYS-Fluent software and 2D steady-state simulations using computational fluid dynamics to determine the effect of unlined spillway surface irregularities (height and angle) on hydraulic parameters. The study focused on how changes to irregularity height and angle affected flow velocity, dynamic pressure, static pressure, total pressure, shear stress, velocity head, pressure head, elevation, energy, and energy loss. The findings revealed that:

(1) Irregularities affected hydraulic parameters, despite existing approaches for determining hydraulic erosive parameters not considering these irregularities.
(2) Velocity at a constant height did not continually decrease as α_1 increased, and these changes were often negligible.
(3) Changes in irregularity angle had a minimal effect on maximum flow velocity at greater heights; however, altering irregularity height had a marked effect.

(4) Holding the irregularity angle constant, total pressure along the channel bottom decreased as h increased. At a constant h, however, total pressure did not consistently decrease as α_1 increased; these latter changes were typically negligible. At greater heights, changes in angle had a minimal impact on total pressure; however, altering irregularity height had a marked effect.
(5) Total pressure, using maximum dynamic pressure to determine the total pressure, increased 2.5–3× relative pressure along the channel bottom.
(6) Along the water–rock interface, 70% of the energy was lost along the profile.
(7) Energy at the water–rock interface increased by approx. 30% upstream and 250%–350% downstream.
(8) Increased flow velocity increased energy and decreased energy loss.

It should be noted that the 2D nature of this research represented a limitation. Additionally, the simulations were steady-state and not time-dependent (transient). Furthermore, the effect of geometric characteristics of the unlined spillway, i.e., overall spillway profile and length, was not considered in this study. Future research should address these limitations to provide a more comprehensive understanding of the subject.

5. Conclusions

In conclusion, this study undertook a comprehensive assessment of the influence exerted by unlined spillway surface irregularities on key hydraulic parameters. The findings unveiled a discernible impact of irregularities on static, dynamic, and total pressures, as well as maximum flow velocity, shear stress, and energy distribution. It is important to acknowledge that, while the study successfully examined the effect of surface irregularities, the broader interaction between spillway geometry and hydraulic parameters still requires further exploration. The utilization of a 2D modeling approach proved instrumental in integrating irregularity effects into the evaluation of erosive hydraulic parameters. Nevertheless, it is essential to recognize that the current investigation encountered certain limitations, primarily stemming from its 2D nature and steady-state simulations. The study's focus on irregularities leaves room for subsequent research to encompass the broader influence of geometric characteristics, such as overall spillway profile and length, to provide a more comprehensive and nuanced understanding of the subject matter. This study significantly contributes to the evolving discourse surrounding hydraulic parameters in the context of unlined spillways, paving the way for future investigations to address remaining intricacies and offer practical insights.

Author Contributions: Conceptualization, Y.J.K.; methodology, Y.J.K. and A.S.; software, Y.J.K.; validation, Y.J.K., A.S., M.-I.F. and J.P.; formal analysis, Y.J.K.; investigation, Y.J.K.; resources, Y.J.K. and A.S.; writing original draft preparation, Y.J.K.; writing, review and editing, Y.J.K., A.S., M.-I.F. and J.P.; visualization, Y.J.K., A.S., M.-I.F. and J.P.; supervision, A.S., M.-I.F.; industrial advising, J.P.; project administration, A.S.; funding acquisition, A.S. All authors have read and agreed to the published version of the manuscript.

Funding: This research was funded by: Natural Sciences and Engineering Research Council of Canada and Hydro-Québec (NSERC, Hydro-Quebec) [CRDPJ 537350-18]. Natural Sciences and Engineering Research Council of Canada (NSERC) [RGPIN-2019-06693].

Institutional Review Board Statement: Not applicable.

Informed Consent Statement: Not applicable.

Data Availability Statement: Not applicable.

Acknowledgments: The authors would like to thank the organizations that have funded this project: Natural Sciences and Engineering Research Council of Canada (NSERC) and Hydro-Quebec, and all those who helped us to improve the quality of this review.

Conflicts of Interest: The authors declare that they have no conflicts of interest regarding the content of this document.

References

1. Pells, S. *Erosion of Rock in Spillways*; University Of New South Wales: New South Wales, Sydney, 2016.
2. Rock, A.J. *Semi-Empirical Assessment of Plunge Pool Scour: Two-Dimensional Application of Annandale's Erodibility Index Method on four Dams in British Columbia, Canada, A. Colorado School of Mines*; Arthur Lakes Library: Golden, CO, USA, 2015.
3. Jalili Kashtiban, Y.; Saeidi, A.; Farinas, M.-I.; Quirion, M. A Review on Existing Methods to Assess Hydraulic Erodibility Downstream of Dam Spillways. *Water* **2021**, *13*, 3205. [CrossRef]
4. Blake, W.; Hedley, D.G. *Rockbursts: Case Studies from North American Hard-Rock Mines*; SME: Southfield, MI, USA, 2003.
5. Saeidi, A.; Eslami, E.; Quirion, M.; Seifaddini, M. Assessment of rock mass erosion in unlined spillways using developed vulnerability and fragility functions. *Georisk Assess. Manag. Risk Eng. Syst. Geohazards* **2020**, *14*, 280–292. [CrossRef]
6. Annandale, G. Erodibility. *J. Hydraul. Res.* **1995**, *33*, 471–494. [CrossRef]
7. Annandale, G.W. Current Technology to Predict Scour of Rock. In *Golden Rocks 2006, The 41st US Symposium on Rock Mechanics (USRMS)*; OnePetro: Richardson, TX, USA, 2006.
8. Kirsten, H.A.; Moore, J.S.; Kirsten, L.H.; Temple, D.M. Erodibility criterion for auxiliary spillways of dams. *Int. J. Sediment Res.* **2000**, *15*, 93–107.
9. Moore, J.S.; Temple, D.M.; Kirsten, H.A. Headcut advance threshold in earth spillways. *Bull. Assoc. Eng. Geol.* **1994**, *31*, 277–280.
10. Van Schalkwyk, A. Minutes—Erosion of rock in unlined spillways. *ICOLD Q* **1994**, *71*, 1056–1062.
11. Bollaert, E.; Schleiss, A. *Transient Water Pressures in Joints and Formation of Rock Scour Due to High-Velocity Jet Impact*; EPFL-LCH: Lausanne, Switzerland, 2002.
12. Bollaert, E. The Comprehensive Scour Model: Theory and Feedback from Practice. In Proceedings of the 5th International Conference on Scour and Erosion, San Francisco, CA, USA, 7–10 November 2010.
13. Carlotti, P. Two-point properties of atmospheric turbulence very close to the ground: Comparison of a high resolution LES with theoretical models. *Bound. Layer Meteorol.* **2002**, *104*, 381–410. [CrossRef]
14. Schmidt, H.; Schumann, U. Coherent structure of the convective boundary layer derived from large-eddy simulations. *J. Fluid Mech.* **1989**, *200*, 511–562. [CrossRef]
15. Townsend, A. *The Structure of Turbulent Shear Flow*; Cambridge university press: Cambridge, UK, 1976.
16. Darcy, H. *Recherches Expérimentales Relatives au Mouvement de l'eau Dans les Tuyaux*; Mallet-Bachelier: Paris, France, 1857; Volume 1.
17. Weisbach, J.L. *Lehrbuch der Ingenieur-und Maschinen-Mechanik: Theoretische Mechanik*; Druck und Verlag von Friedrich Vieweg und Sohn: Braunschweig, Gemary, 1845; Volume 1.
18. Manning, R.; Griffith, J.P.; Pigot, T.; Vernon-Harcourt, L.F. *On the Flow of Water in Open Channels and Pipes*; Transaction of the Institution of Civil Engineers of Ireland: Dublin, Ireland, 1890; Volume 20.
19. Yunus, A.C. *Fluid Mechanics: Fundamentals And Applications (Si Units)*; Tata McGraw Hill Education Private Limited: New York, NY, USA, 2010.
20. Khodashenas, S.R.; Paquier, A. A geometrical method for computing the distribution of boundary shear stress across irregular straight open channels. *J. Hydraul. Res.* **1999**, *37*, 381–388. [CrossRef]
21. Prasad, B.V.R.; Russell, M.J. Discussion of "Diffusional Mass Transfer at Sediment-Water Interface" by Nancy Steinberger and Midhat Hondzo. *J. Environ. Eng.* **2000**, *126*, 576. [CrossRef]
22. Yang, S.-Q.; Lim, S.-Y. Boundary shear stress distributions in trapezoidal channels. *J. Hydraul. Res.* **2005**, *43*, 98–102. [CrossRef]
23. Guo, J.; Julien, P.Y. Shear stress in smooth rectangular open-channel flows. *J. Hydraul. Eng.* **2005**, *131*, 30–37. [CrossRef]
24. Seckin, G.; Seckin, N.; Yurtal, R. Boundary shear stress analysis in smooth rectangular channels. *Can. J. Civ. Eng.* **2006**, *33*, 336–342. [CrossRef]
25. Severy, A.; Felder, S. Flow Properties and Shear Stress on a Flat-Sloped Spillway. In Proceedings of the 37th IAHR World Congress, Kuala Lumpur, Malaysia, 13–18 August 2017; pp. 13–18.
26. Kashtiban, Y.J.; Shahriar, K.; Bakhtavar, E. Assessment of blasting impacts on the discontinuities in a salt stope and pillar mine using a developed image processing. *Bull. Eng. Geol. Environ.* **2022**, *81*, 1–14. [CrossRef]
27. Lopez Jimeno, C. *Drilling and Blasting of Rocks*; A.A. Balkema: Rotterdam, The Netherlands; Brookfield, VT, USA, 1995.
28. Fluent, A. 12.0 Theory Guide. *Ansys Inc* **2009**, *5*, 15.
29. Hirt, C.W.; Nichols, B.D. Volume of fluid (VOF) method for the dynamics of free boundaries. *J. Comput. Phys.* **1981**, *39*, 201–225. [CrossRef]
30. Bombardelli, F.A.; Hirt, C.; García, M.H.; Matthews, B.; Fletcher, C.; Partridge, A.; Vasquez, S. Computations of curved free surface water flow on spiral concentrators. *J. Hydraul. Eng.* **2001**, *127*, 629–631. [CrossRef]
31. Lee, C.-H.; Xu, C.; Huang, Z. A three-phase flow simulation of local scour caused by a submerged wall jet with a water-air interface. *Adv. Water Resour.* **2019**, *129*, 373–384. [CrossRef]
32. Imanian, H.; Mohammadian, A. Numerical simulation of flow over ogee crested spillways under high hydraulic head ratio. *Eng. Appl. Comput. Fluid Mech.* **2019**, *13*, 983–1000. [CrossRef]
33. Li, Y.; Gao, Y.; Jia, X.; Sun, X.; Zhang, X. Numerical Simulations of Hydraulic Characteristics of A Flow Discharge Measurement Process with A Plate Flowmeter in A U-Channel. *Water* **2019**, *11*, 2382. [CrossRef]